



ELSEVIER

Contents lists available at ScienceDirect

Chemical Engineering Journal

journal homepage: www.elsevier.com/locate/cej



BiOBr_xI_{1-x}/BiOBr heterostructure engineering for efficient molecular oxygen activation

Yang Bai^a, Xian Shi^a, Pingquan Wang^{a,*}, Li Wnag^b, Kai Zhang^a, Ying Zhou^a, Haiquan Xie^b, Jinan Wang^c, Liqun Ye^{a,b,*}

^a State Key Laboratory of Oil and Gas Reservoir Geology and Exploitation, School of Oil & Natural Gas Engineering, Southwest Petroleum University, Chengdu 610500, China

^b Engineering Technology Research Center of Henan Province for Solar Catalysis, Collaborative Innovation Center of Water Security for Water Source Region of Mid-line of South-to-North Diversion Project of Henan Province, College of Chemistry and Pharmaceutical Engineering, Nanyang Normal University, Nanyang 473061, China

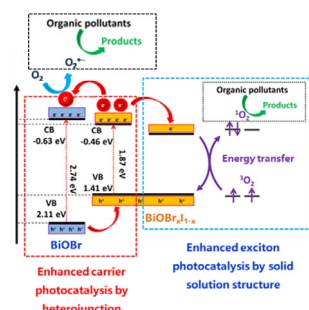
^c ESIQIE, Instituto Politecnico Nacional, col Zacatenco, Mexico City 07738, Mexico

HIGHLIGHTS

- # BiOBr_xI_{1-x}/BiOBr heterostructure was in-situ synthesized.
- # BiOBr_xI_{1-x}/BiOBr showed effective activity for wastewater treatment.
- # Exciton and carrier photocatalytic processes was found.

GRAPHICAL ABSTRACT

The both enhanced excitation and carrier photocatalysis of BiOBr/BiOBr_xI_{1-x} resulted efficient molecular oxygen activation for oilfield waste water treatment and organic pollutants (BPA, RhB and phenol) photodegradation.



ARTICLE INFO

Keywords:

BiOBr_xI_{1-x}/BiOBr
Molecular oxygen activation
Synergistic effect
Environmental remediation

ABSTRACT

The BiOBr_xI_{1-x}/BiOBr heterojunction structural photocatalyst was constructed successfully in this work and it was formed by the BiOBr_xI_{1-x} solid solution coupling with the BiOBr monomer, which was determined by efficient characterizations. For the photocatalytic property, The BiOBr_xI_{1-x}/BiOBr could degrade some organic pollutants efficiently and the oilfield produced waste water treatment efficiency of it was ideal. The reason for its enhanced photocatalytic property was also explored. Through ESR tests, trapping experiments and other efficient methods, the enhanced molecular oxygen activation capacity of induced ¹O₂ and O₂^{•-} photogeneration by BiOBr_xI_{1-x} solid solution structure and heterostructure in one photocatalyst was confirmed, respectively. This work provided a new thought for enhanced molecular oxygen activation capacity of bismuth oxyhalide photocatalysts.

1. Introduction

Photocatalysis has been recognized as an efficient technology for

environmental remediation [1–4]. The species to which oxygen transformed with high reactivity are generally regarded as reactive oxygen species (ROS), which can degrade the organic pollutants non-

* Corresponding authors at: Southwest Petroleum University, Nanyang Normal University, China.

E-mail addresses: baizhangyq@foxmail.com (P. Wang), yeliqun@163.com (L. Ye).

<https://doi.org/10.1016/j.cej.2018.09.006>

Received 29 May 2018; Received in revised form 27 August 2018; Accepted 2 September 2018

Available online 03 September 2018

1385-8947/ © 2018 Elsevier B.V. All rights reserved.

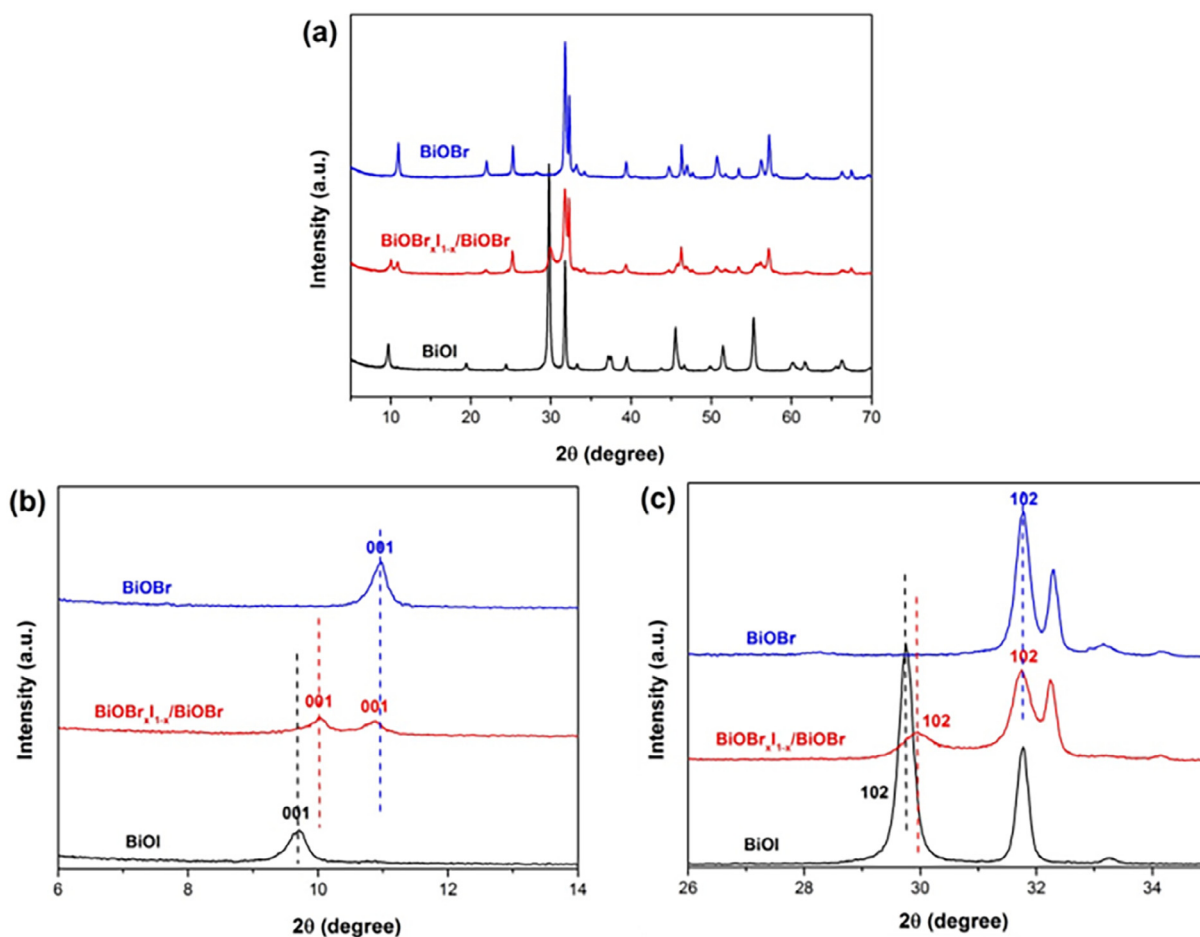


Fig. 1. XRD patterns of BiOBr, BiOBr_xI_{1-x}/BiOBr and BiOI: (a) 5–70°, (b) 6–14°, and (c) 26–35°.

selectively. So, superior photocatalytic degradation performance of a photocatalyst usually depends on the amount and type of the photo-generated ROS, which is also called molecular oxygen activation capacity. In addition, the analysis of the ROS is also important for understanding the photocatalytic mechanism. While, the ROS speciationability is usually determined by the molecular oxygen activation of the photocatalysts. Photocatalysts with high quality can possess excellent molecular oxygen activation capacity under light illumination [5,6]. Therefore, improving the activation capacity of molecular oxygen has become an important factor that should be considered when designing the photocatalytic materials [7,8].

As a kind of efficient strategies for enhanced molecular oxygen activation capacity, forming modified structural photocatalysts have been reported in many researches. Herein, we intend to take bismuth oxyhalide (BiOX (X = Br and I)) as the basic material for further improving the photocatalytic molecular oxygen activation under visible light [9]. In view of the BiOX, the enhanced molecular oxygen activation capacity can be reached by forming solid solution structure and heterostructure according to previous reports [10,11]. In general, through the efficient measurement of the O₂^{•−}, more generation of the O₂^{•−} indicates the enhanced molecular oxygen activation capacity by carrier photocatalysis. Besides the O₂^{•−}, it has been verified that exciton photocatalytic process of BiOBr photocatalyst also occurred, which was confirmed by the generation of the singlet oxygen (¹O₂) [12–14]. In our previous work, we had demonstrated that the exciton and carrier photocatalysis could be enhanced by forming BiOBr_{0.5}I_{0.5} solid solution and BiOBr/BiOI heterojunction, respectively. The enhanced molecular oxygen activation capacity under visible light was approved by the characterizations of the amount and type of the ROS. More ¹O₂

generated by BiOBr_{0.5}I_{0.5} solid solution and more O₂^{•−} generated by BiOBr/BiOI heterojunction illustrated the enhanced molecular oxygen activation capacity of these two photocatalysts, respectively [15]. Therefore, the molecular oxygen activation capacity can be improved by the modified structures formation of the BiOX (X = Br and I). If the solid solution and heterojunction structures are formed in one BiOX photocatalytic material at the same time, the molecular oxygen activation capacity might be further enhanced. There are many reports for the BiOBr_xI_{1-x} solid solution and BiOBr/BiOI heterostructure, respectively [16,17]. However, a photocatalyst formed by BiOX monomer coupled with the BiOBr_xI_{1-x} has been rarely researched.

Bearing this mind, we firstly in-situ synthesised the BiOBr_xI_{1-x}/BiOBr photocatalyst. Through the efficient characterizations we determined the photocatalyst was formed by BiOBr_xI_{1-x} and BiOBr. Through the ESR tests we intuitively confirmed the enhanced molecular oxygen activation ability for both O₂^{•−} and ¹O₂. Due to the enhanced molecular oxygen activation capacity of BiOBr_xI_{1-x}/BiOBr, the ideal efficiency of organic pollutants degradation and oilfield waste water treatment had been achieved. The photocatalytic mechanism of the improved molecular oxygen activation capacity of BiOBr_xI_{1-x}/BiOBr was also explored and explained. This work provided a new thought for enhanced the molecular oxygen activation ability of bismuth oxyhalide photocatalysts.

2. Experimental

2.1. Materials

Bi(NO₃)₃·5H₂O, KBr, KI, ethylene glycol (EG) were of analytical

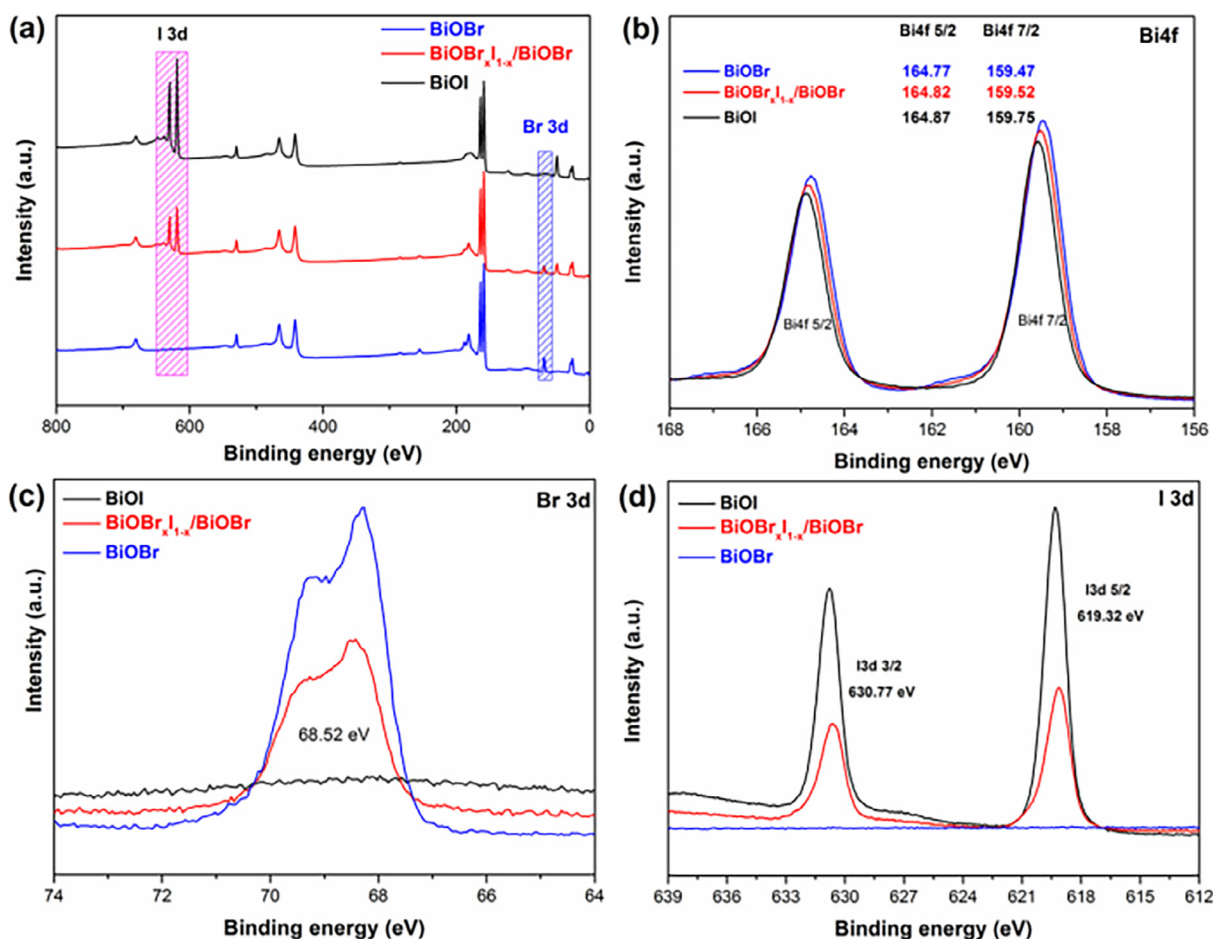


Fig. 2. XPS spectra of BiOI, BiOBr and BiOBr_xI_{1-x}/BiOBr: (a) survey, (b) Bi 4f, (c) Br 3d, and (d) I 3d.

reagent grade without further purification. The deionized water was prepared by water purification system and used throughout the whole experiments.

2.2. Synthesis

Different from the synthesis methods of the BiOBr_xI_{1-x} in previous reports, we added the I and Br sources in separation. The amount of KBr and KI were calculated firstly with different molar Br : I ratios of 2:0, 1.5:0.5 and 0:2 (the total amount of KBr and KI was 1 mmol). 1 mmol of Bi(NO₃)₃·5H₂O and a certain amount of KBr were dissolved in 20 mL of deionized water and stirred for 30 min firstly. After the suspension formed, 20 mL of an ethylene glycol (EG) solution containing a certain amount of KI was added dropwise. The precipitates were collected after continuous stirring for 2 h. The precipitates were washed repeatedly with deionized water and dried at 80 °C for 10 h.

2.3. Characterization

The phase and crystal structures of as-prepared samples were characterized by X-ray diffraction (XRD) on a Bruker D8 diffractometer using Cu Kα (λ = 1.5406) radiation in a 2θ range from 5° to 70°. The morphology and structure of the as-prepared samples were observed using a Sigma Zeiss Field emission scanning electron microscopy (FESEM). Transmission electron microscopy (TEM) images were measured by a FEI Tecnai G20 transmission electron microscopy with selected area electron diffraction (SAED). UV–vis diffuse reflectance spectroscopy (DRS) was obtained by a UV–vis spectrometer (Perkin Elmer, Lambda 650 s, BaSO₄ as a reference) and record on the within

the region of 200–800 nm. X-ray photoelectron spectroscopy (XPS) was determined by a Thermo ESCALAB 250XI x-ray photoelectron spectroscopy. Time-resolved PL spectra recorded by a FLS920 Multifunction Steady State and Transient State Fluorescence Spectrometer (Edinburgh Instruments, room temperature).

2.4. Photocatalytic tests

Pollutants degradation: The target degradation compounds were Rhodamine B(RhB), Phenol and Bisphenol A (BPA). The Photo-degradation was under visible-light using a 300-W Xe lamp with a UV-cutoff filter (λ > 400 nm). 0.05 g of photocatalyst was suspended in a 100 mL aqueous solution of 20 mg L⁻¹ RhB, 10 mg L⁻¹ Phenol and 10 mg L⁻¹ BPA, respectively. Before illumination, the suspensions were magnetically stirred in dark for 40 min to ensure the establishment of an adsorption-desorption equilibrium between the photocatalysts and pollutants. Then, the UV–vis adsorption spectrum of the centrifuged solution was recorded using a UV–vis spectrophotometer.

Oilfield produced wastewater treatment: oilfield produced waste water was sampled from the production site of the PetroChina Southwest Oil & Gasfield Company. 0.1 g of photocatalysts was suspended in a 100 mL oilfield produced wastewater. Before illumination, the suspensions were magnetically stirred in dark for 1 h to ensure the establishment of an adsorption-desorption equilibrium between the photocatalysts and organics in the wastewater. The whole photocatalytic wastewater treatment was under a 300-W Xe lamp without a UV-cutoff filter for 5 h, and the water was sampled and the COD value was measured per hour.

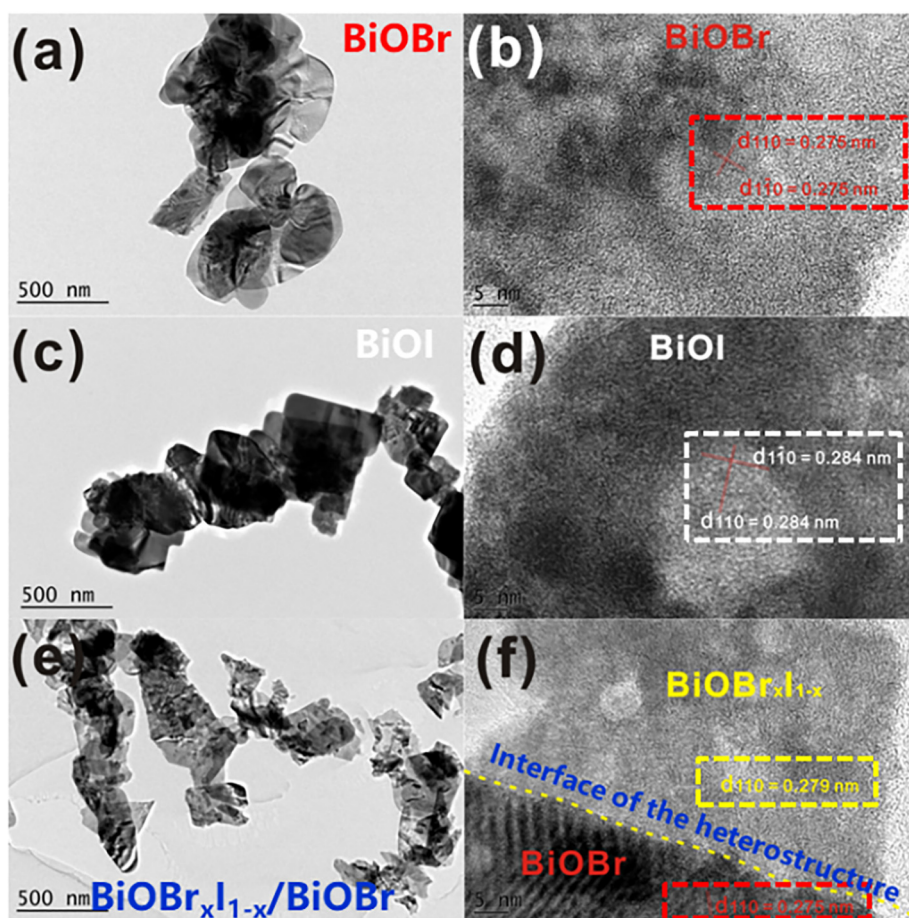


Fig. 3. TEM and HRTEM images of BiOBr (a) and (b); BiOI (c) and (d); BiOBr_xI_{1-x}/BiOBr (e) and (f).

2.5. COD measurements

1 mL of waste water was diluted to 100 times in a volumetric flask firstly. 2.5 mL diluent was measured by a burette and poured into a test tube. Then 1.5 mL solution Y (prepared by 90 mL distilled water + 10 mL concentrated sulfuric acid + 2.5 g K₂Cr₂O₇) was added dropwise by another burette and shook the mixed liquor up. Measured 5 mL of solution C (prepared by 100 mL concentrated sulfuric acid + 1 g Ag₂SO₄), added into the above mixed liquor dropwise and shook for about 10 min. Put the test tube in a digester under 160 °C for 15 min. The solution was cooled to room temperature and the COD value was measured by a water analyzer.

2.6. Reactive oxygen species (ROS) quantification experiments

Nitrotetrazolium blue chloride (NBT, 2.5×10^{-5} mol L⁻¹, exhibiting an absorption maximum at 259 nm) and 3,3',5,5'-tetramethylbenzidine (TMB, 0.1 g L⁻¹, exhibiting an absorption maximum at 380 nm) were used to determine the amount of photocatalytic O₂^{•-} and ¹O₂ generation. 10 mg of photocatalysts were added into 50 mL NBT aqueous and sampling ever 10 min; 1 mg of photocatalysts was added 16 mL HAc/NaAc buffer solution (pH = 3.6) and 4 mL distilled water, then 2 mg TMB was added in and sampling every 3 min. Both of them were stirred under a xenon lamp. The production of O₂^{•-} was quantitatively analysed by detecting the concentration of NBT and ¹O₂ was analysed by the oxidation rate of TMB with a UV-vis spectrophotometer [18,19].

2.7. ESR tests

50 μL of aqueous suspension of samples (2 mg L⁻¹) was mixed with 500 μL of 2,2,6,6-tetramethylpiperidine nitrogen oxide solution (TEMP, 50×10^{-3} mol L⁻¹). After being illuminated for 5 min, the mixture was characterized using a Bruker EMX plus model spectrometer operating at the X-band frequency (9.4 GHz) at room temperature for ¹O₂ test. The O₂^{•-} trapping ESR tests were also performed as described above, except the use of 5,5-Dimethyl-1-pyrroline N-oxide (DMPO, 50×10^{-3} mol L⁻¹) as the spin-trapping agent. A xenon lamp (50 W) was used as the light source [20].

2.8. Photoelectrochemical measurement

Electrochemical impedance spectra (EIS) and transient photocurrent responses of the prepared samples were tested by a CHI660D electrochemical working station (CHI Instruments, Shanghai, China) in a three-electrode quartz cell with Na₂SO₄ (0.1 mol L⁻¹) electrolyte solution. Samples were deposited on a fluorinated-tin-oxide (FTO) conducting glass as the working electrode, Ag/AgCl and Pt were used as the reference and the counter electrodes, respectively.

3. Results and discussion

Fig. 1 showed the XRD patterns of BiOBr, BiOBr_xI_{1-x}/BiOBr and BiOI. BiOI and BiOBr displayed a series of diffraction peaks in agreement with the standard XRD patterns, respectively (PDF: 01-073-2062 (BiOI) and 01-085-0862 (BiOBr)) [21,22]. Fig. 1(b) and (c) displayed the enlarged XRD patterns for comparing and distinguishing the diffraction peaks of BiOBr_xI_{1-x}/BiOBr. For (001) peaks, the peak at

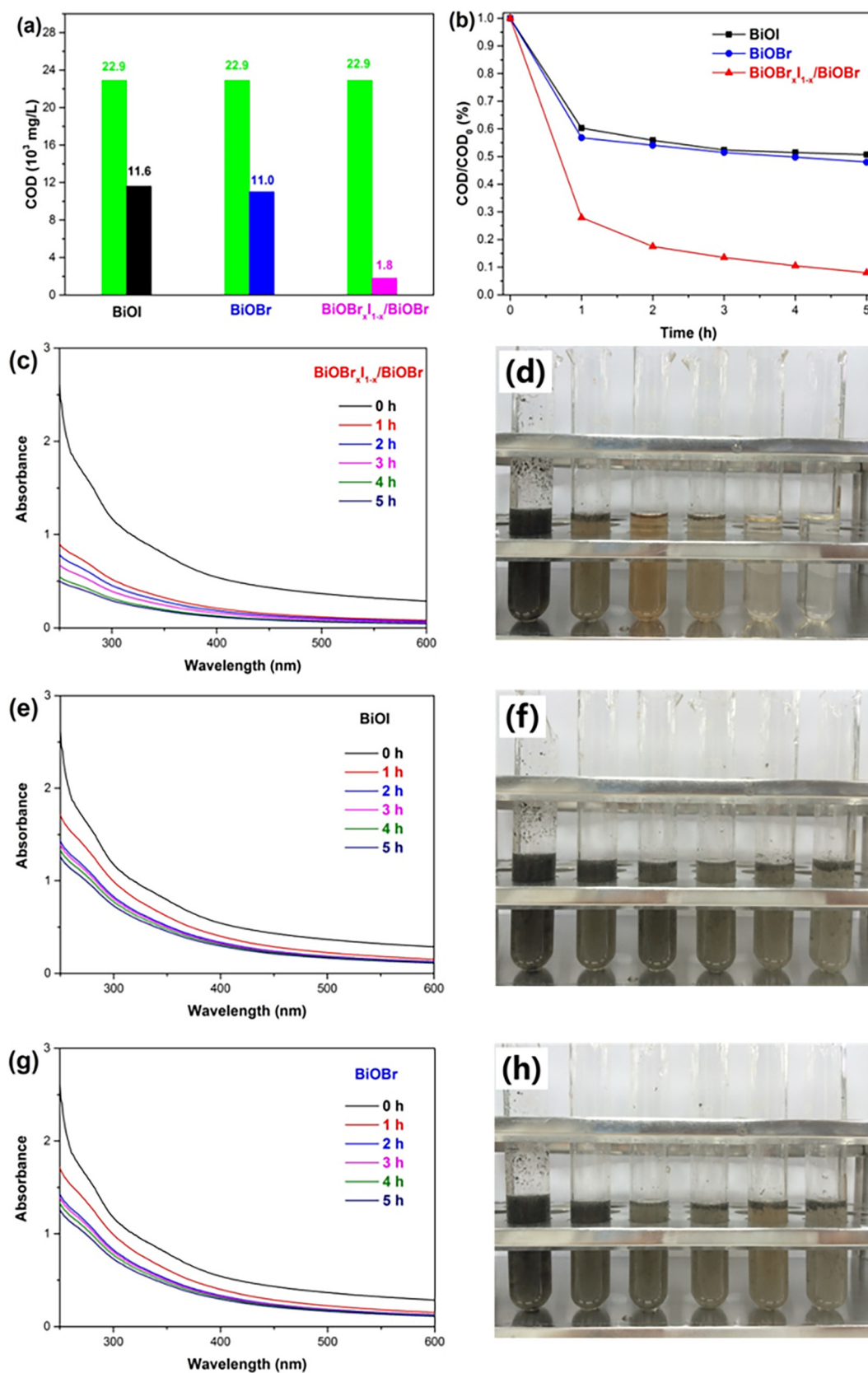


Fig. 4. COD values of original oilfield produced wastewater and after treatment by BiOI, BiOBr, and BiOBr_xI_{1-x}/BiOBr (a); COD reduction rates of BiOI, BiOBr, and BiOBr_xI_{1-x}/BiOBr treatments (b); temporal absorption spectra of oilfield wastewater over the BiOBr_xI_{1-x}/BiOBr (c) BiOI (e) and BiOBr (g) under full wavelength irradiation treatment; actual photos of oilfield wastewater after 0 h, 1 h, 2 h, 3 h, 4 h, 5 h treatment over BiOBr_xI_{1-x}/BiOBr (d), BiOI (f) and BiOBr (h).

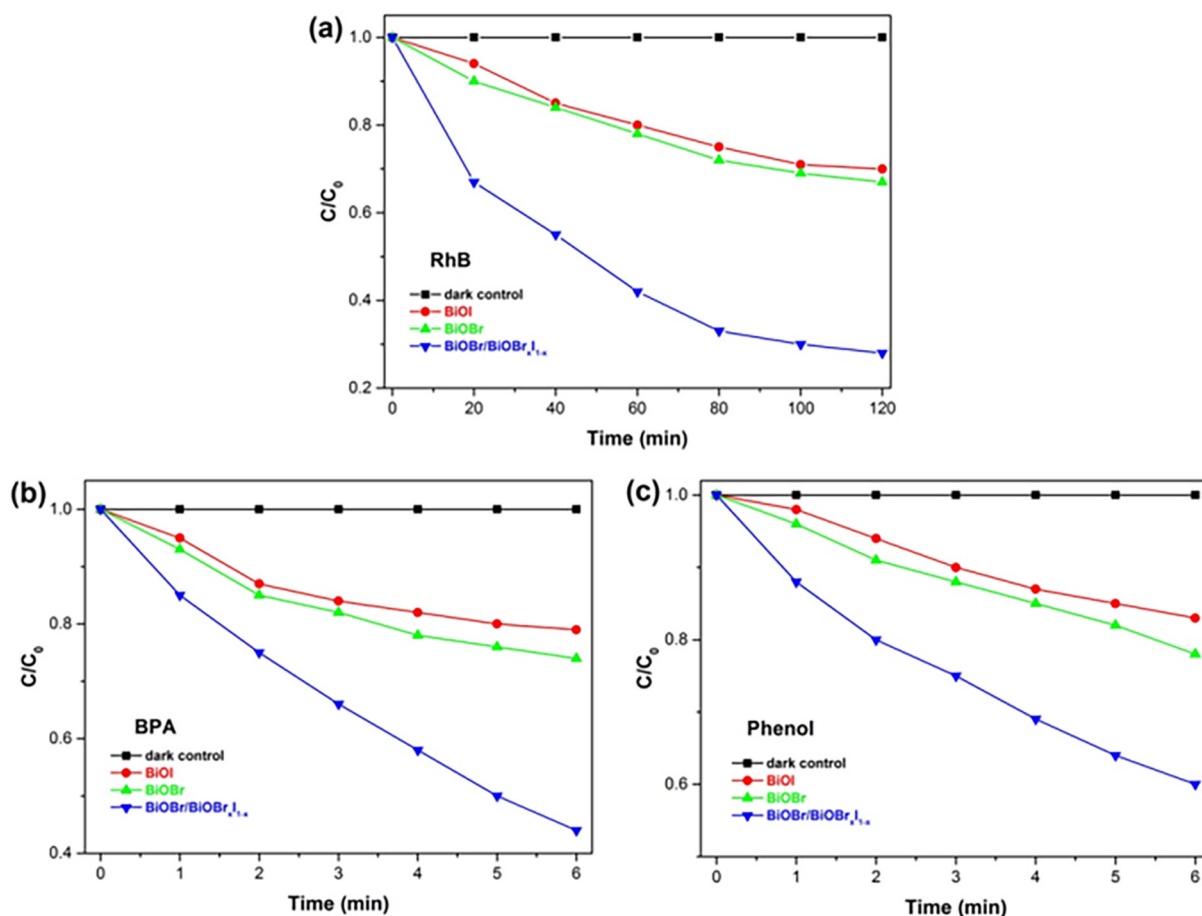


Fig. 5. Photocatalytic activities of $\text{BiOBr}_x\text{I}_{1-x}/\text{BiOBr}$ and BiOX ($X = \text{Br}, \text{I}$) for RhB degradation (a); Phenol degradation (b) and BPA degradation (c) under visible light irradiation.

$2\theta = 9.99^\circ$ of the $\text{BiOBr}_x\text{I}_{1-x}/\text{BiOBr}$ was new formed and its position was between the (001) peaks of BiOI and BiOBr , which was in agreement with that of $\text{BiOBr}_x\text{I}_{1-x}$. For the peak at $2\theta = 10.86^\circ$ of $\text{BiOBr}_x\text{I}_{1-x}/\text{BiOBr}$, it was at the same position as that of BiOBr . The two (001) peaks of $\text{BiOBr}_x\text{I}_{1-x}/\text{BiOBr}$ indicated $\text{BiOBr}_x\text{I}_{1-x}$ was coupled with BiOBr and $\text{BiOBr}_x\text{I}_{1-x}/\text{BiOBr}$ was formed successfully. The same phenomenon of (102) and (012) peaks were also observed in Fig. 1(c). The peaks at 31.81° and 29.91° matched well with the (102) peaks of $\text{BiOBr}_x\text{I}_{1-x}$ and BiOBr , respectively. So it could be confirmed the formation of the $\text{BiOBr}_x\text{I}_{1-x}/\text{BiOBr}$ heterostructure by $\text{BiOBr}_x\text{I}_{1-x}$ and BiOBr from the XRD patterns intuitively.

XPS was used to analyse the element contents of $\text{BiOBr}_x\text{I}_{1-x}/\text{BiOBr}$. The survey spectrum (Fig. 2(a)) showed $\text{BiOBr}_x\text{I}_{1-x}/\text{BiOBr}$ was consisted by the Bi, O, Br and I elements, and high purity of the prepared samples was also indicated. Fig. 2(b) showed the $\text{Bi } 4f_{7/2}$ and $\text{Bi } 4f_{5/2}$ peaks of $\text{BiOBr}_x\text{I}_{1-x}/\text{BiOBr}$ were at 159.27 eV and 164.57 eV, suggesting that the existence of Bi^{3+} . The banding energy of 68.52 eV was corresponding to $\text{Br } 3d$ (Fig. 2(c)), and the banding energies of 619.32 eV and 630.77 eV were corresponding to $\text{I } 3d_{5/2}$ and $\text{I } 3d_{3/2}$ (Fig. 2(d)), which was associated with Br^- and I^- , respectively. The comparison of the UV-vis DRS spectra of BiOI , BiOBr and $\text{BiOBr}_x\text{I}_{1-x}/\text{BiOBr}$ were shown in Fig. S1. BiOI and BiOBr had fundamental adsorption edges at 665.1 nm and 436.3 nm, respectively. After the BiOBr coupling with $\text{BiOBr}_x\text{I}_{1-x}/\text{BiOBr}$, it showed adsorption edges at 614.9 nm. The experimental results indicated that all samples could be excited by visible light.

The TEM and HRTEM patterns of BiOBr , BiOI and $\text{BiOBr}_x\text{I}_{1-x}/\text{BiOBr}$ were expounded in Fig. 3 and all the samples expressed the same architecture and size. For pure BiOX ($X = \text{Br}$ and I), the interplanar

spacing of $\{110\}$ planes of BiOBr and BiOI were 0.276 nm and 0.284 nm, which was in accordance with standard values, respectively [23]. As for $\text{BiOBr}_x\text{I}_{1-x}/\text{BiOBr}$, there was a boundary in Fig. 3(f) (yellow line) implied the BiOBr coupled with $\text{BiOBr}_x\text{I}_{1-x}$ clearly. In addition, it could be found that two groups interplanar spacing data of (110) planes were in the $\text{BiOBr}_x\text{I}_{1-x}/\text{BiOBr}$ sample. The new formed (110) planes (0.279 nm) was of the $\text{BiOBr}_x\text{I}_{1-x}$, while the standard (110) planes 0.276 nm was of pure BiOBr respectively, which were in agreement with previous reports, respectively [23]. So it could be concluded from the Fig. 3 that the $\text{BiOBr}_x\text{I}_{1-x}/\text{BiOBr}$ heterostructure was formed visually and it was in accordance with above XRD and XPS experimental results.

Herein, the $\text{BiOBr}_x\text{I}_{1-x}/\text{BiOBr}$ photocatalyst was used for the actual oilfield produced wastewater treatment, and BiOX ($X = \text{Br}, \text{I}$) were as the contrast groups (Fig. 4). As was shown in Fig. 4(a) and (b), $\text{BiOBr}_x\text{I}_{1-x}/\text{BiOBr}$ expressed superior effect for oilfield produced wastewater treatment and it could reduce the COD value from 22900 mg L^{-1} to 1800 mg L^{-1} in 5 h, the COD reduction rate was almost 2 times than that of BiOX ($X = \text{Br}, \text{I}$). The temporal absorption spectra (Fig. 4(d), (f) and (h)) showed the absorption curves of waste water in 5 h treatment. $\text{BiOBr}_x\text{I}_{1-x}/\text{BiOBr}$ showed the obviously maximum decline than that of BiOX ($X = \text{Br}, \text{I}$), which was in agreement with best efficiency of oilfield produced wastewater treatment. From the Fig. 4(c), (e) and (g) it could be observed from the photos that the colour of the wastewater treated by $\text{BiOBr}_x\text{I}_{1-x}/\text{BiOBr}$ after 5 h was much clearer than that of the BiOX ($X = \text{Br}, \text{I}$), which was also in agreement with the experimental results visually.

Besides the oilfield waste water treatment, we also found that the $\text{BiOBr}_x\text{I}_{1-x}/\text{BiOBr}$ heterostructure photocatalyst could also enhance the

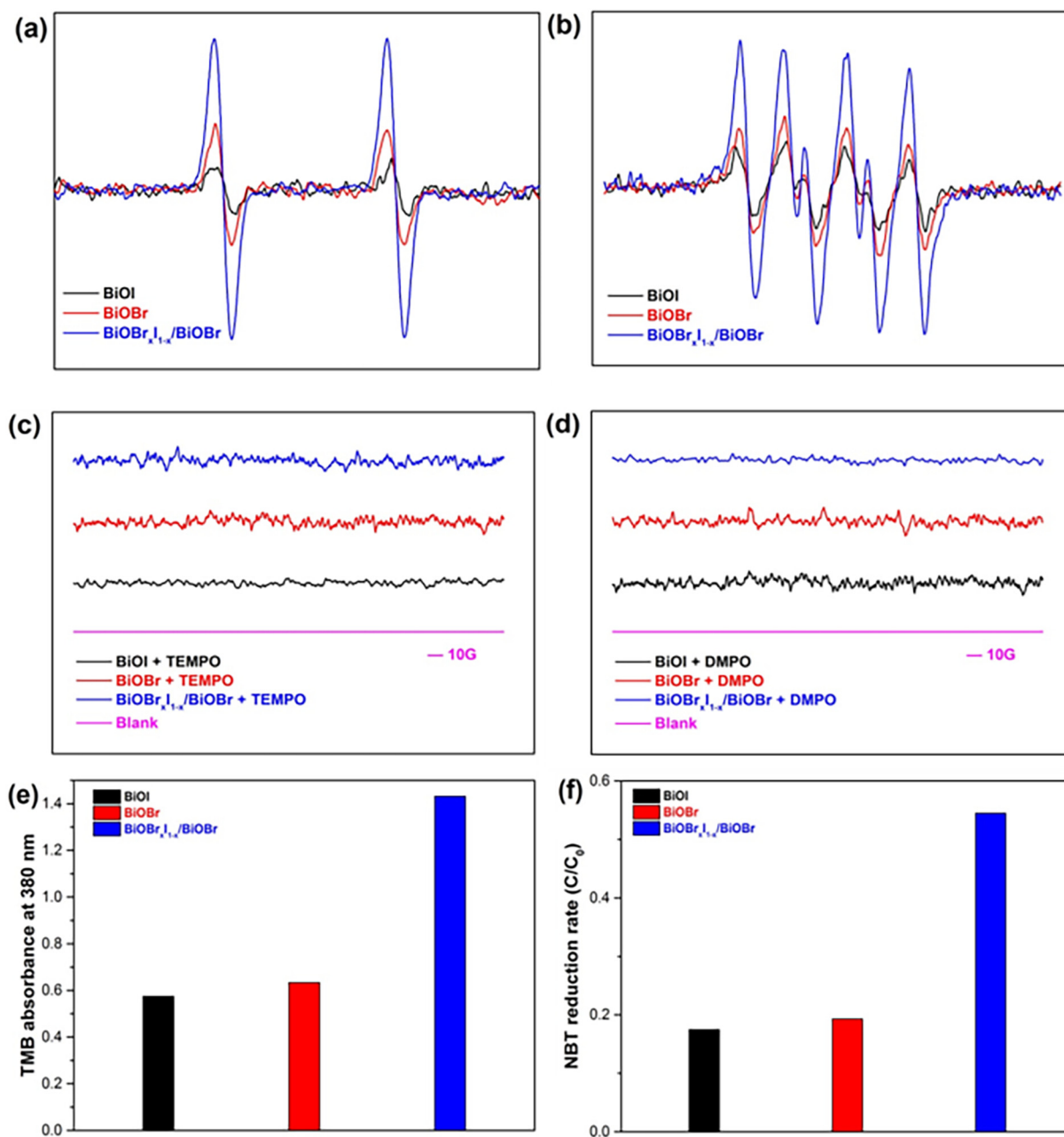


Fig. 6. ESR tests of singlet oxygen (a) and superoxide radical (b); controlled experiments of ESR tests for singlet oxygen (c) and superoxide radical (d) without light irradiation; total absorbance of TMB oxidation (e) and total reduction rates of NBT (f) after 15 min visible light irradiation.

photocatalytic properties for some organic pollutants degradation. In this part, the target degradation compounds were Rhodamine B (RhB), Phenol and Bisphenol A (BPA), respectively. The photocatalytic degradation rates of BiOBr_xI_{1-x}/BiOBr were shown in Fig. 5 and were compared with BiOBr and BiOI. As were shown in Fig. 5(a), (b) and (c), BiOBr_xI_{1-x}/BiOBr expressed best photocatalytic degradability of all these three organic pollutants than BiOI and BiOBr, it removed about 80% of RhB, 40% of Phenol and 60% BPA under 120 min irradiation, respectively, which were 2 times than that of BiOX (X = Br, I). From the wastewater treatment and photocatalytic activities experimental results, we concluded that BiOBr_xI_{1-x}/BiOBr enhanced the photocatalytic performance exactly, and we explored the enhanced photocatalytic mechanisms of BiOBr_xI_{1-x}/BiOBr next step.

We explored the enhanced molecular oxygen activation ability for both O₂^{•−} and ¹O₂ of BiOBr_xI_{1-x}/BiOBr next step. As was mentioned

earlier, ¹O₂ and O₂^{•−} were the typical ROS generated by exciton and carrier photocatalysis, respectively. So, herein, we regarded ¹O₂ and O₂^{•−} as the target reactive oxygen species for both molecular oxygen activation ability and the photocatalytic mechanisms exploration. And ESR, which was confirmed as the most direct evidence for different generated ROS, was used for the photocatalytic exploration [24–27]. In Fig. 6(a) and (b), the both strongest ¹O₂ and O₂^{•−} signals of BiOBr_xI_{1-x}/BiOBr indicated the better ability of ¹O₂ and O₂^{•−} generation than BiOX (X = Br, I). Control experiments by adding quenchers (Fig. 6(c) and (d)) were also finished for verifying ESR results. Meanwhile, 3, 3', 5, 5'-tetramethylbenzidine (TMB, adsorption peak at 380 nm) and Nitrotetrazolium blue chloride (NBT, adsorption peak at 259 nm) were used to evaluate the generation of ¹O₂ and O₂^{•−} and the experimental results (Fig. 6(e) and (f)) expressed the same phenomenon as the ESR tests [28–31]. We measured molecular oxygen activation

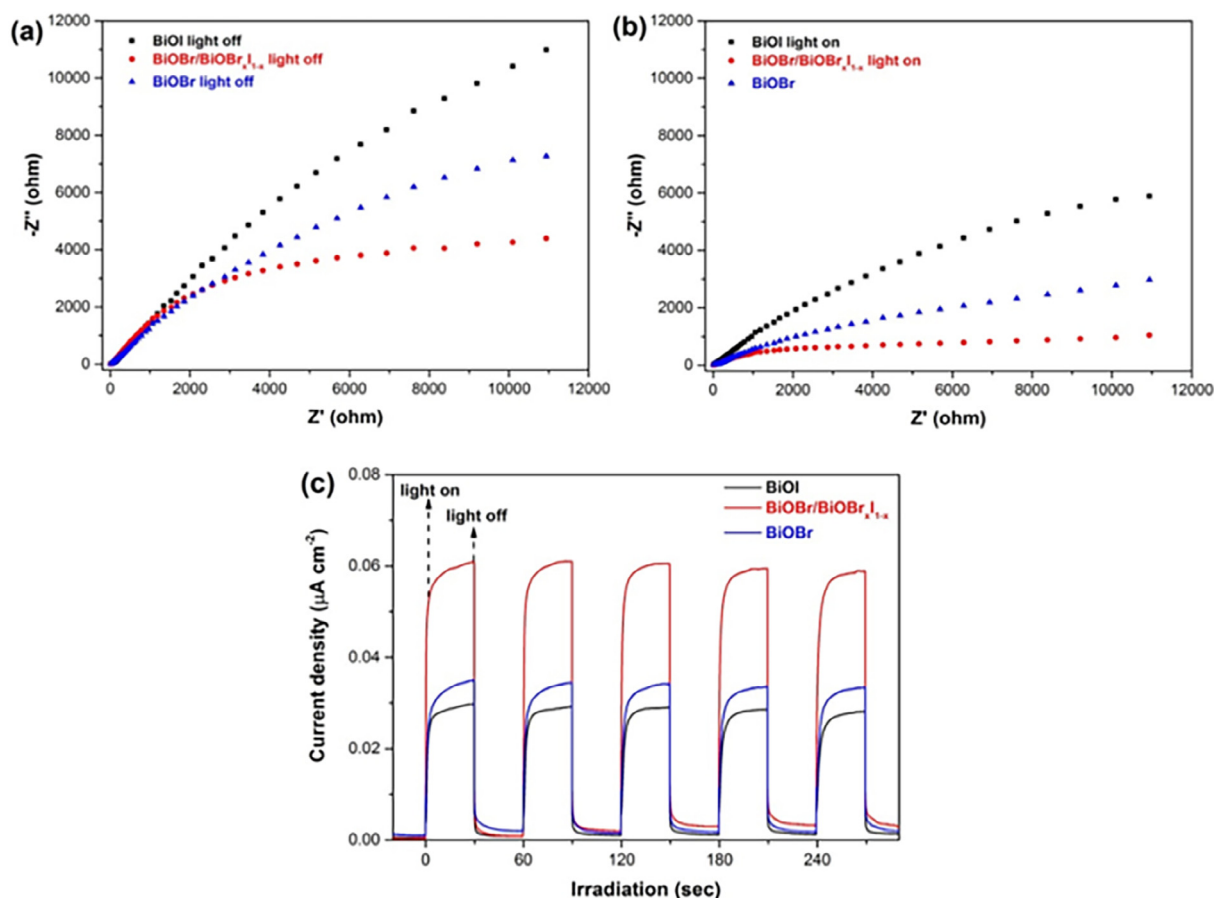
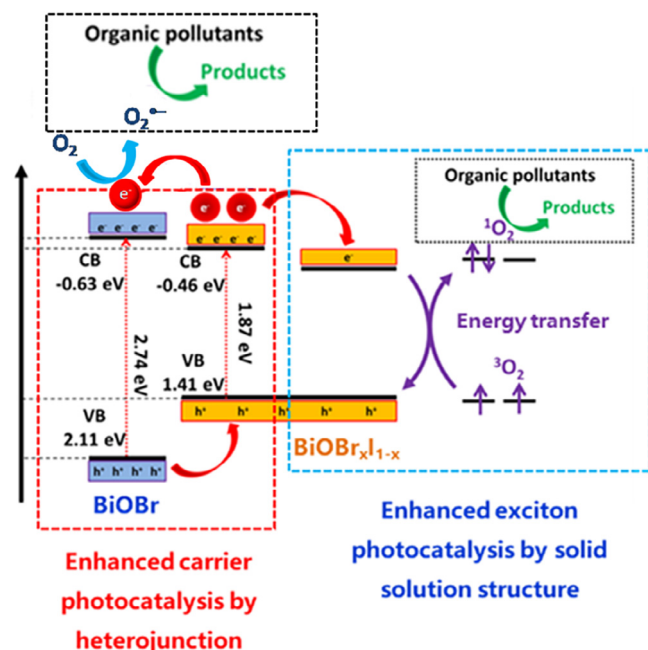


Fig. 7. EIS experimental results (a) and (b); Photocurrent (c) of $\text{BiOBr}_x\text{I}_{1-x}/\text{BiOBr}$ and BiOX ($X = \text{Br}, \text{I}$).



Scheme 1. Enhanced exciton and carrier photocatalytic mechanisms of $\text{BiOBr}_x\text{I}_{1-x}/\text{BiOBr}$.

properties of BiOI , $\text{BiOBr}/\text{BiOBr}_{x-1-x}$ and BiOBr by using NBT and TMB as probe molecules, as shown in Fig. S2. Compared with BiOI and BiOBr , $\text{BiOBr}/\text{BiOBr}_{x-1-x}$ revealed largest oxidation and reduction rate of TMB and NBT, respectively, indicated that the both enhanced exciton

and carrier photocatalytic mechanisms clearly.

The carrier photocatalysis could be determined by electrochemical experiments [21,32]. For verifying the same enhanced carrier photocatalytic mechanism as exciton photocatalysis of $\text{BiOBr}_x\text{I}_{1-x}/\text{BiOBr}$, the electrochemical impedance and photocurrent response spectra of $\text{BiOBr}_x\text{I}_{1-x}/\text{BiOBr}$ and BiOX ($X = \text{Br}, \text{I}$) were compared and shown in Fig. 7. $\text{BiOBr}_x\text{I}_{1-x}/\text{BiOBr}$ expressed a semicircle arc with a smaller diameter than BiOX ($X = \text{Br}, \text{I}$) (Fig. 7(a) and (b)) and showed that the $\text{BiOBr}_x\text{I}_{1-x}/\text{BiOBr}$ had lower resistance value for electron-transfer than BiOX ($X = \text{Br}, \text{I}$). And also, as shown in Fig. 7(c), $\text{BiOBr}_x\text{I}_{1-x}/\text{BiOBr}$ revealed a much higher photocurrent than BiOX ($X = \text{Br}, \text{I}$). The experimental results in this part clarified the enhanced carrier photocatalysis of $\text{BiOBr}_x\text{I}_{1-x}/\text{BiOBr}$. So, it could be concluded that the induced molecular oxygen activation capacity was supported by both enhanced carrier and exciton photocatalytic mechanisms of $\text{BiOBr}_x\text{I}_{1-x}/\text{BiOBr}$.

The enhanced exciton and carrier photocatalytic mechanisms scheme of $\text{BiOBr}_x\text{I}_{1-x}/\text{BiOBr}$ was shown as following. As shown in Scheme 1, for the enhanced carrier photocatalysis, the electrons of $\text{BiOBr}_x\text{I}_{1-x}$ were activated up to its CB position and then transferred to the CB of BiOBr due to the heterojunction. Accordingly, photo-induced electrons on the surface of BiOBr could be trapped by O_2 to form $\text{O}_2^{\cdot-}$, which became a reactive species for organic pollutants degradation [33,34]. Meanwhile, the unique layered structure of $\text{BiOBr}_x\text{I}_{1-x}$ solid solution possessed intensive electron-hole interactions and promoted exciton photocatalysis process due to the photo-generated holes of BiOBr transferred to $\text{BiOBr}_x\text{I}_{1-x}$ where singlet oxygen generation via energy transfer during this process was confirmed, and a lot of singlet oxygen generated during this process support its excellent photocatalytic properties [35–37].

4. Conclusion

In this work, we successfully in-situ synthesized the BiOBr/BiOBr_xI_{1-x} heterostructure photocatalysts and witnessed its excellent molecular oxygen activation ability through efficient characterization results. The improved photocatalytic efficiency for oilfield waste water treatment and organic pollutants degradation also proved above result. Besides, through the analysis of ROS, the both enhanced exciton and carrier photocatalytic mechanisms were also verified. The induced amount of the photogenerated ¹O₂ and O₂^{•-} were due to the enhanced excitation and carrier photocatalysis, which were promoted by the solid solution structure and heterostructure of BiOBr/BiOBr_xI_{1-x}, respectively. The enhanced molecular activation of BiOBr/BiOBr_xI_{1-x} supported the excellent water treatment capacity and organic pollutants degradability when it was inspired by light.

Acknowledgments

This work was supported by the National Natural Science Foundation of China (No. 51502146, 51872147, 51702270, 21671113), the Program for Innovative Research Team of Science and Technology in the University of Henan Province (19IRTSTHN025), Petro China Innovation Foundation (2018D-5007-0604), and Open Fund (201601) of State Key Laboratory of Physical Chemistry of Solid Surfaces (Xiamen University).

Appendix A. Supplementary data

Supplementary data associated with this article can be found, in the online version, at <https://doi.org/10.1016/j.cej.2018.09.006>.

References

- C. Boix, M. Ibáñez, J.V. Sancho, J.R. Parsons, P. Voogt, F. Hernández, Biotransformation of pharmaceuticals in surface water and during waste water treatment: Identification and occurrence of transformation products, *J. Hazard. Mater.* 302 (2015) 175–187.
- S.K. Chatterjee, I. Bhattacharjee, G. Chandra, Biosorption of heavy metals from industrial waste water by *Geobacillus thermodenitrificans*, *J. Hazard. Mater.* 175 (2010) 117–125.
- A. Bhatnagar, M. Sillanpää, Utilization of agro-industrial and municipal waste materials as potential adsorbents for water treatment—a review, *Chem. Eng. J.* 157 (2010) 277–296.
- F. Tou, Y. Yi, J. Feng, Z. Niu, P. Hui, Y. Qin, X. Guo, X.Z. Meng, L. Min, M.F. Hochella, Environmental risk implications of metals in sludges from waste water treatment plants: the discovery of vast stores of metal-containing nanoparticles, *Environ. Sci. Technol.* 51 (2017) 4831–4840.
- T. Mano, S. Nishimoto, Y. Kameshima, M. Miyake, Water treatment efficacy of various metal oxide semiconductors for photocatalytic ozonation under UV and visible light irradiation, *Chem. Eng. J.* 264 (2015) 221–229.
- M. Martín-Sómer, B. Vega, C. Pablos, R.V. Grieken, J. Marugán, Wavelength dependence of the efficiency of photocatalytic processes for water treatment, *Appl. Catal. B* 221 (2017) 258–265.
- Q. Zheng, D.P. Durkin, J.E. Elenewski, Y. Sun, N.A. Banek, L. Hua, H. Chen, M.J. Wagner, W. Zhang, D. Shuai, Visible-light-responsive graphitic carbon nitride: rational design and photocatalytic applications for water treatment, *Environ. Sci. Technol.* 50 (2016) 12938–12948.
- R. Hao, G. Wang, H. Tang, L. Sun, C. Xu, D. Han, Template-free preparation of macro/mesoporous g-C₃N₄/TiO₂ heterojunction photocatalysts with enhanced visible light photocatalytic activity, *Appl. Catal. B* 187 (2016) 47–58.
- Y. Bai, T. Chen, P. Wang, L. Wang, L. Ye, Bismuth-rich Bi₄O₅X₂ (X = Br, and I) nanosheets with dominant 101 facets exposure for photocatalytic H₂ evolution, *Chem. Eng. J.* 304 (2016) 454–460.
- Y. Bai, L. Ye, L. Wang, X. Shi, P. Wang, W. Bai, P.K. Wong, g-C₃N₄/Bi₄O₅I₂ heterojunction with I³⁻/I⁻ redox mediator for enhanced photocatalytic CO₂ conversion, *Appl. Catal. B* 194 (2016) 98–104.
- L. Ye, X. Jin, C. Liu, C. Ding, H. Xie, K.H. Chu, P.K. Wong, Thickness-ultrathin and bismuth-rich strategies for BiOBr to enhance photoreduction of CO₂ into solar fuels, *Appl. Catal. B* 187 (2016) 281–290.
- C.Y. Wang, X. Zhang, X.N. Song, W.K. Wang, H.Q. Yu, Novel Bi₁₂O₁₅Cl₆ photocatalyst for the degradation of bisphenol A under visible-light irradiation, *ACS Appl. Mater. Interfaces* 8 (2016) 5320–5326.
- J.C. Ahern, R. Fairchild, S.T. Jin, J. Carr, H.H. Patterson, Characterization of BiOX compounds as photocatalysts for the degradation of pharmaceuticals in water, *Appl. Catal. B* 179 (2015) 229–238.
- A. Henríquez, H.D. Mansilla, J. Freer, D. Contreras, Selective oxofunctionalization of cyclohexane over titanium dioxide-based and bismuth oxyhalide (BiOX, X = Cl⁻, Br⁻, I⁻) photocatalysts by visible light irradiation, *Appl. Catal. B* 206 (2017) 252–262.
- A. Dandapat, H. Gnyam, Y. Sasson, The fabrication of BiOClxBr 1-x/alumina composite films with highly exposed 001 facets and their superior photocatalytic activities, *Chem. Commun.* 52 (2015) 2161–2164.
- H. Wang, S. Chen, D. Yong, X. Zhang, S. Li, W. Shao, X. Sun, B. Pan, Y. Xie, Giant electron-hole interactions in confined layered structures for molecular oxygen activation, *J. Am. Chem. Soc.* 139 (2017) 4737–4742.
- Y. Bai, X. Shi, P. Wang, H. Xie, L. Ye, Photocatalytic Mechanism regulation of bismuth oxyhalogen via changing atomic assembly method, *ACS Appl. Mater. Interfaces* 9 (2017) 30273–30277.
- H. Wang, S. Jiang, S. Chen, D. Li, X. Zhang, W. Shao, X. Sun, J. Xie, Z. Zhao, Q. Zhang, Enhanced singlet oxygen generation in oxidized graphitic carbon nitride for organic synthesis, *Adv. Mater.* 28 (2016) 6940–6945.
- J. Park, D. Feng, S. Yuan, H.C. Zhou, Photochromic metal-organic frameworks: reversible control of singlet oxygen generation, *Angew. Chem. Int. Ed.* 54 (2015) 430–435.
- J. Schmitt, V. Heitz, A. Sour, F. Bolze, H. Ftouni, J.F. Nicoud, L. Flamigni, B. Ventura, Diketopyrrolopyrrole-porphyrin conjugates with high two-photon absorption and singlet oxygen generation for two-photon photodynamic therapy, *Angew. Chem.-Int. Ed.* 54 (2015) 169–173.
- M. Shang, W.Z. Wang, L. Zhang, Preparation of BiOBr lamellar structure with high photocatalytic activity by CTAB as Br source and template, *J. Hazard. Mater.* 167 (2009) 803–809.
- L. Ye, X. Jin, X. Ji, C. Liu, Y. Su, H. Xie, C. Liu, Facet-dependent photocatalytic reduction of CO₂ on BiO nanosheets, *Chem. Eng. J.* 29 (2016) 39–46.
- Z. Jia, F. Wang, F. Xin, B. Zhang, Simple solvothermal routes to synthesize 3D BiOBr_xI_{1-x} microspheres and their visible-light-induced photocatalytic properties, *Ind. Eng. Chem. Res.* 50 (2011) 6688–6694.
- X. Xiao, ZuoX HaoR, J. Nan, L. Li, W. Zhang, Microwave-assisted synthesis of hierarchical Bi₂O₃I₃ microspheres for efficient photocatalytic degradation of bisphenol-A under visible light irradiation, *Chem. Eng. J.* 209 (2012) 293–300.
- F.T. Li, Q. Wang, X.J. Wang, B. Li, Y.J. Hao, R.H. Liu, D.S. Zhao, In-situ one-step synthesis of novel BiOCl/Bi₂₄O₃₁Cl₁₀ heterojunctions via self-combustion of ionic liquid with enhanced visible-light photocatalytic activities, *Appl. Catal. B* 150–151 (2014) 574–584.
- W.J. Kim, D. Pradhan, B.K. Min, Y. Sohn, Adsorption/photocatalytic activity and fundamental natures of BiOCl and BiOCl_xI_{1-x} prepared in water and ethylene glycol environments, and Ag and Au-doping effects, *Appl. Catal. B* 147 (2014) 711–725.
- H. Cheng, B. Huang, X. Qin, X. Zhang, Y. Dai, A controlled anion exchange strategy to synthesize Bi₂S₃ nanocrystals/BiOCl hybrid architectures with efficient visible light photoactivity, *Chem. Commun.* 48 (2011) 97–99.
- J. Xiao, Y. Xie, Q. Han, H. Cao, Y. Wang, F. Nawaz, F. Duan, Superoxide radical-mediated photocatalytic oxidation of phenolic compounds over Ag⁺/TiO₂: Influence of electron donating and withdrawing substituents, *J. Hazard. Mater.* 304 (2016) 126–133.
- H. Huang, X. Han, X. Li, S. Wang, P.K. Chu, Y. Zhang, Fabrication of multiple heterojunctions with tunable visible-light-active photocatalytic reactivity in BiOBr-BiOI full-range composites based on microstructure modulation and band structures, *ACS Appl. Mater. Interfaces* 7 (2015) 482–492.
- E. Díez-Mato, F.C. Cortezón-Tamarit, S. Bogialli, D. García-Fresnadillo, M.D. Marazuela, Phototransformation of model micropollutants in water samples by photocatalytic singlet oxygen production in heterogeneous medium, *Appl. Catal. B* 160–161 (2014) 445–455.
- M. Pan, H. Zhang, Liu L GaoG, W. Chen, Facet-dependent catalytic activity of nanosheets-assembled BiOI microspheres in degradation of bisphenol a, *Environ. Sci. Technol.* 49 (2015) 6240–6248.
- Y. Nosaka, A.Y. Nosaka, Generation and detection of reactive oxygen species in photocatalysis, *Chem. Rev.* 117 (2017) 11302–11336.
- C. Schweitzer, R. Schmidt, Physical mechanisms of generation and deactivation of singlet oxygen, *Chem. Rev.* 103 (2003) 1685–1757.
- J.A. Rengifo-Herrera, K. Pierzchala, A. Sienkiewicz, L. Forró, J. Kiwi, C. Pulgarin, Abatement of organics and *Escherichia coli* by N, S co-doped TiO₂ under UV and visible light. Implications of the formation of singlet oxygen (¹O₂) under visible light, *Appl. Catal. B: Environ.* 88 (2009) 398–406.
- I. Fenoglio, J. Ponti, E. Alloa, M. Ghiazza, I. Corazzari, R. Capomaccio, D. Rembges, S. Oliaro-Bosso, F. Rossi, Singlet oxygen plays a key role in the toxicity and DNA damage caused by nanometric TiO₂ in human keratinocytes, *Nanoscale* 5 (2013) 6567–6576.
- C. Santaella, B. Allainmat, F. Simonet, J. Labille, M. Auffan, J. Rose, W. Achouak, Aged TiO₂-based nanocomposite used in sunscreens produces singlet oxygen under long-wave UV and sensitizes *Escherichia coli* to cadmium, *Environ. Sci. Technol.* 48 (2014) 5245–5253.
- N.M. Dimitrijevic, E. Rozhkova, T. Rajh, Dynamics of localized charges in dopamine-modified TiO₂ and their effect on the formation of reactive oxygen species, *J. Am. Chem. Soc.* 131 (2009) 2893–2899.

Update

Chemical Engineering Journal

Volume 359, Issue , 1 March 2019, Page 813

DOI: <https://doi.org/10.1016/j.cej.2018.11.002>



Contents lists available at ScienceDirect

Chemical Engineering Journal

journal homepage: www.elsevier.com/locate/cej



Corrigendum

Corrigendum to “BiOBr_xI_{1-x}/BiOBr heterostructure engineering for efficient molecular oxygen activation” [Chem. Eng. J. 365 (2019) 34–42]



Yang Bai^a, Xian Shi^a, Pingquan Wang^{a,*}, Li Wnag^b, Kai Zhang^a, Ying Zhou^a, Haiquan Xie^b, Jin An Wang^c, Liqun Ye^{a,b,*}

^a State Key Laboratory of Oil and Gas Reservoir Geology and Exploitation, School of Oil & Natural Gas Engineering, Southwest Petroleum University, Chengdu 610500, China

^b Engineering Technology Research Center of Henan Province for Solar Catalysis, Collaborative Innovation Center of Water Security for Water Source Region of Mid-line of South-to-North Diversion Project of Henan Province, College of Chemistry and Pharmaceutical Engineering, Nanyang Normal University, Nanyang 473061, China

^c ESIQIE, Instituto Politécnico Nacional, Col Zacatenco, Mexico City 07738, Mexico

The authors regret that the author “Jinan Wang” and his affiliation contain errors. Now the corrected name and affiliation have been added as shown above.

The authors would like to apologize for any inconvenience caused by this regard.

* Corresponding authors at: Southwest Petroleum University, Nanyang Normal University, China.

DOI of original article: <https://doi.org/10.1016/j.cej.2018.09.006>

<https://doi.org/10.1016/j.cej.2018.11.002>